Korean J. Chem. Eng., 40(4), 1014-1022 (2023)
DOI: 10.1007/s11814-022-1366-y

pISSN: 0256-1115
eISSN: 1975-7220

Impedimetric sensing platform based on copper oxide with activated carbon for sensitive detection of amoxicillin

Muhammad Tajmeel Feroze, Dulyawat Doonyapisut, Byeongkyu Kim, and Chan-Hwa Chung†

School of Chemical Engineering, Sungkyunkwan University, Suwon 16419, Korea
(*Received 27 July 2022 • Revised 20 November 2022 • Accepted 4 December 2022*)

Abstract−Copper oxide with activated carbon-based materials was synthesized for the selective detection of amoxicillin (AMX) in aqueous samples. The morphological and structural characteristics of the materials were evaluated using a scanning electron microscope and X-ray diffraction. Electrochemical impedance spectroscopy and voltammetric techniques were also used to observe the electrochemical response of the system. The best AMX sensing behavior was obtained with the presence of copper oxide that interacts with AMX and the increased surface area of activated carbon, which results in a sharp oxidation current. The electrode showed two linear responses in the AMX concentration ranges from 10 μM to 100 μM and from 1 mM to 5 mM, respectively. In the linear ranges, the sensitivity of the sensing materials was calculated to be 9.5528 Ω μM^{-1} and 0.14994 Ω μM^{-1}, respectively. The statistical test confirms that the electrode showed good repeatability and selectivity in the determination of AMX.

Keywords: Electrochemical Sensor, Copper Oxide, Amoxicillin, Electrochemical Impedance Spectroscopy

INTRODUCTION

Since the discovery of the antibiotic penicillin by Alexander Fleming in 1928, it has been used to treat and prevent a wide range of human and infectious diseases [1]. Molecules that possess beta-lactam rings are generally considered penicillins [2]. The third generation of penicillin was found to be significantly effective against a larger variety of gram-negative and gram-positive bacteria [3]. Among these, amoxicillin (AMX) is one of the most commonly prescribed antibiotics in this category to treat and prevent a wider range of diseases, which includes otitis, pneumonia, and infections of the ear, throat, and other parts of the skin [4-6]. Its applications are also found in veterinary medicines for treating and curing diseases in animals [7]. Harmful effects, however, have been reported including nausea, vomiting, rashes, spermatogenesis, central nervous system disorder, and antibiotic-related colitis [8,9]. Nevertheless, It has been categorized as an important antimicrobial drug for humans by World Health Organization (WHO) [10].

Much attention has been devoted to controlling it with the increasing concern of pollutants in the environment. Though these drugs are prepared under strict regulations, their side effects on human and animal health, due to the high discard of such pollutants, cannot be ignored [11,12]. The efflux of antibiotics, particularly AMX, is the main source of contamination in tap water which ultimately leads to risking the health of human, animal, and aquatic life [13,14]. Thus, it is essential to measure and control the AMX concentration at low levels in the water [15]. Numerous analytical techniques have been reported for the separation, quantification, and analyses of AMX, such as HPLC [16,17], UV spectrophotometry [18,19], spectrofluorometry [20], chemiluminescence [21], and microbiological [22] methods. However, these methods require expensive instrumentation and complex pretreatments consuming large sample volume and time [2]. Furthermore, such methods also have some disadvantages, such as low sensitivity, low stability, ample quantity of pure organic solvents, and optimization of experimental parameters such as flow rate, mobile phase, and derivative treatment [23-25]. Hence, exploring new methods and developing novel catalytic materials for the detection and analysis of drugs in the shortest time is essential. On the contrary, electrochemical techniques with the advantages of simplicity, high selectivity and sensitivity, fast response, easy operation, cost-effectiveness, and the possibility of miniaturization have received remarkable attention in recent decades for the detection of AMX and other pharmaceutical compounds [26-35].

The results of the antibiotic's breakdown by metal ions, according to earlier investigations, were necessary for the identification of AMX [19]. Here, the antibiotic-metal complex serves as an intermediate in the hydrolytic reaction [36]. Copper cation (Cu^{2+}) has been extensively studied as one of the metal ions that catalyzes the hydrolysis of AMX [19,37]. Various analytical methods have been applied to study the interaction of AMX with copper, but not much attention has been devoted to studying it via electrochemical methods. The unmodified electrodes were also reported previously for the detection of AMX [38,39]. Later, researchers found that electrode surface modification with a suitable modifier was inevitable, to improve the stability, efficiency, and sensitivity of the electrochemical techniques.

Copper oxide (CuO), a transition metal oxide, has emerged as a promising candidate for the detection of pharmaceutical drugs. It possesses distinct features such as superior sensitivity, electrochemical activity, cost-effectiveness, ease of fabrication, and excellent stability in solutions.

†To whom correspondence should be addressed.
E-mail: chchung@skku.edu

In this work, for the preparation of the sensor electrode, Cu powders were annealed at 350 °C for 1 h in a furnace, which resulted in pebble-like copper-oxide powders within the activated carbon on the surface of carbon paper [40-42]. The prepared CuO based electrode has been utilized for the impedimetric detection of AMX. The electrochemical performance of Cu as electrode material in AMX sensing was found to be significantly better than that of other electrodes.

EXPERIMENTAL

1. Materials and Reagents

Amoxicillin (96%) was purchased from Acros Organics (USA). Copper powder (99%) of 14-25 μm in size, monopotassium phosphate (KH_2PO_4), and buffer tablets (pH 7.0) were received from Sigma-Aldrich (USA). Carbon paper was obtained from SGL Carbon (Germany). Dimethylformamide (DMF), sodium chloride (NaCl), potassium chloride (KCl), ammonium chloride (NH_4Cl), calcium chloride ($CaCl_2$), and urea were acquired from Daejung Chemicals (Korea). Copper(II) sulfate pentahydrate was received from Duksan Chemicals (Korea). A freshly prepared stock solution of 0.1 M AMX was prepared each time. Activated carbon (Super-P) was purchased from Alfa Aesar (USA). Polyvinylidene fluoride (PVDF) is acquired from MTI Corp. (China). HCl and NaOH were used in PBS solution to prepare electrolyte of different pH values. During all electrochemical measurements, Deionized (DI) water was used to prepare all electrolyte solutions. DI water was also used throughout the cleaning process.

2. Fabrication of Electrodes

The Cu powders were first annealed in a furnace for 1 h at 350 °C in the presence of air to produce CuO powders [40-42]. A dispersion solution was prepared using annealed Cu powder (70 wt%), activated carbon (15 wt%), and PVDF (10 wt%) as a binder in DMF solution. A tip sonicator was used to disperse the powders in solution for a period of 1 h. After the sonication, the prepared sample was immediately spray-coated on the surface of the carbon-paper substrate (1×1 cm^2) using a spray gun. An amount of 5 mg cm^{-2} is used to coat each electrode. The prepared electrodes were then placed and dried in a vacuum oven for 12 h at 60 °C.

3. Preparation of Synthetic Urine Sample

The synthetic urine sample was prepared using the method proposed by Wong et al. [15]. In a beaker, NaCl, KCl, NH_4Cl, $CaCl_2$, KH_2PO_4, and urea were blended, of which concentration was 49, 20, 18, 10, 15, and 18 mmol L^{-1}, respectively. DI water was also added until the total volume reached 25 mL.

4. Material Characterization

To confirm the electrodes' structure, the prepared electrodes were examined with a field-emission scanning electron microscope (FESEM, JEOL, JSM 7000F). X-ray diffraction equipment (XRD, Bruker, D8 ADVANCE) was also used to examine the crystalline structure of the electrodes in the 2θ range from 20° to 80° at 3° per minute.

5. Electrochemical Measurement

A three-electrode cell was used to conduct the electrochemical measurements under ambient conditions. The reference electrode was Ag/AgCl with 3 M NaCl, and the counter electrode was Pt plate (1×5 cm^2, Nilaco Corp.). The 10 mL buffer solution was used in the electrolyte throughout the experiments. An electrochemical workstation (ZIVE SP1, Won-A Tech, Korea) was used for all electrochemical analyses. The electrochemical impedance spectroscopy (EIS) experiment was performed by applying a potential of +0.15 V (vs. Ag/AgCl) and within a frequency range of 0.1 to 100,000 Hz at an amplitude of 10 mV. AMX was used as an analyte, and a PBS solution of pH 7 was prepared for the experiment.

The electrochemical AMX detection process and EIS model of the CuO@Ac/Cp electrode is exhibited in schematic diagram 1.

RESULTS AND DISCUSSION

1. Morphological and Structure Analysis

Based on the various sample fabrication conditions on carbon paper (Cp) substrates, the samples were named Cp, Ac/Cp, Cu@Ac/

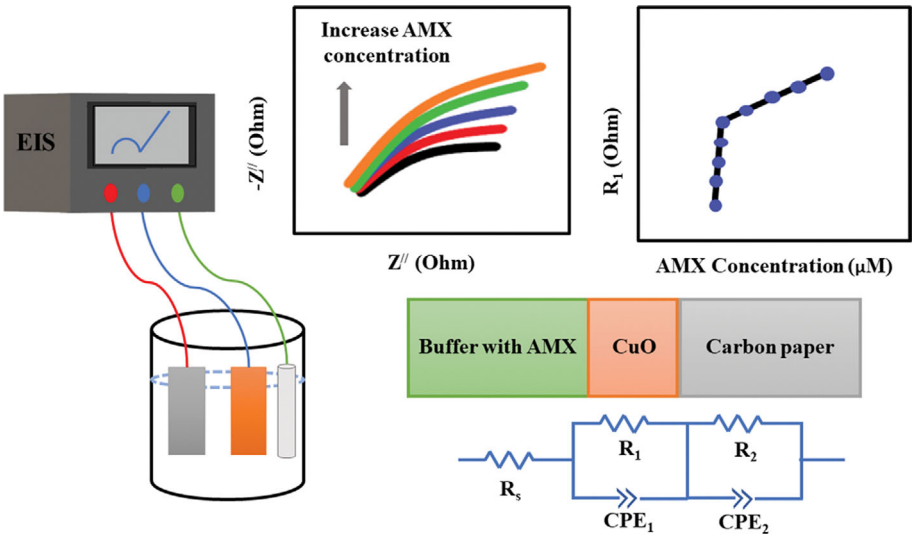

Scheme 1. Schematic illustration of the electrochemical AMX sensor.

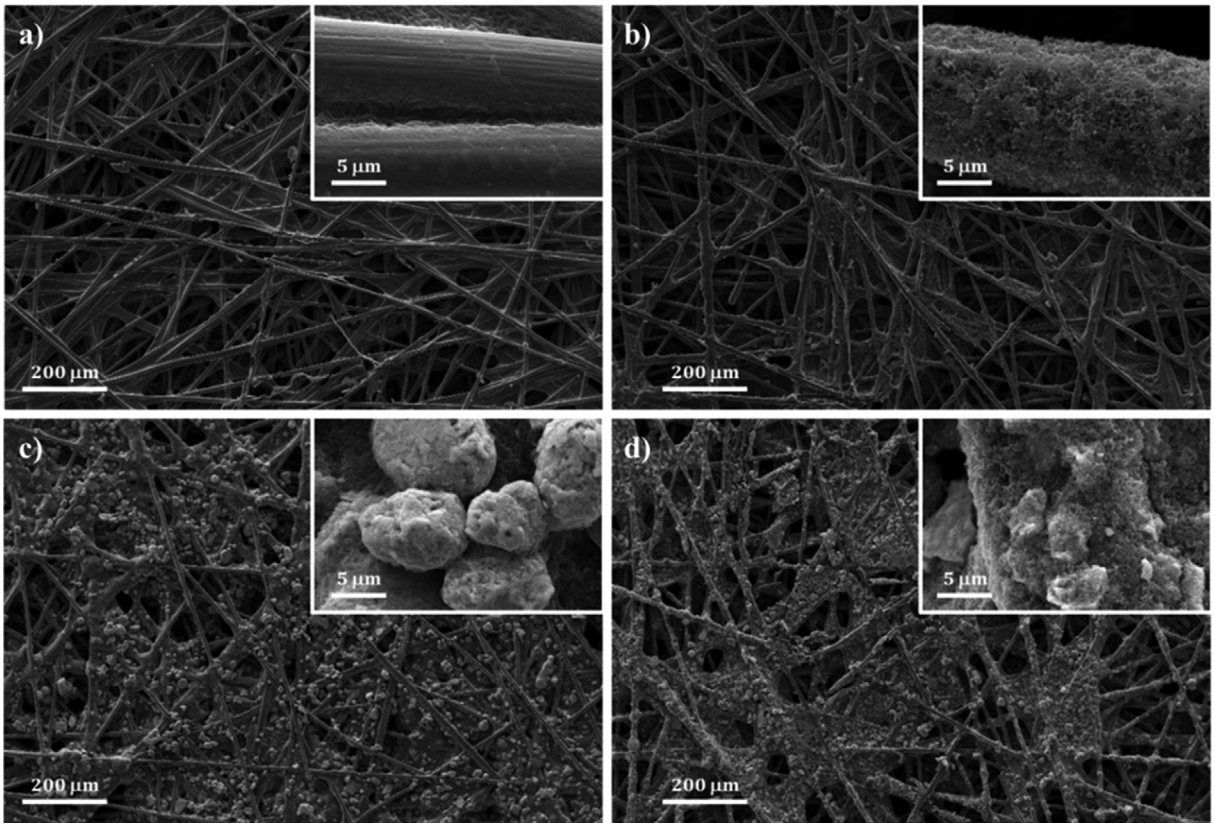

Fig. 1. The FESEM images of (a) bare Cp, (b) Ac/Cp, (c) Cu@Ac/Cp, and (d) CuO@Ac/Cp.

Cp, and CuO@Ac/Cp, respectively, as noted in Table S1. Fig. 1 shows representative FESEM images of the Cu and CuO based electrodes on the surface of carbon paper. In Fig. 1(a)-(b), the web-like structures of bare carbon papers can be seen where the fibers of diameter 5-20 μm are overlapping with each other. The difference between the two samples can be explained in the insets of Fig. 1(a)-(b). Smooth fibers of 5-10 μm can be observed in the inset of Fig. 1(a), whereas much thicker fibers of 10-20 μm are formed in the inset of Fig. 1(b), which indicates the presence of activated carbon on the surface.

In Fig. 1(c)-(d), the Cu@Ac/Cp and the CuO@Ac/Cp look like a web structure having an irregular surface. The surface has some particles of irregular shapes and sizes, which indicate the presence of activated carbons and copper-oxide powders, as presented in the inset of Fig. 1(c)-(d). In both insets of Fig. 1(c)-(d), pebble-like particles can be noticed, which further increases the surface area of electrodes. However, these pebble-like particles are widely distributed in Fig. 1(d), whereas cumulative particles are observed in Fig. 1(c). The synthesized Cu and CuO powders have been characterized by X-ray diffraction, which results are presented in Fig. 2. In Fig. 2(a), the diffraction peaks of (006) and (0012) corresponding to carbons of the carbon paper are evident at 26.6° and 54.8°, respectively. The intensities of those patterns are increased due to the additional deposition of the activated carbon layer on carbon paper as shown in Fig. 2(a). In contrast, as presented in Fig. 2(b), the diffraction peaks of (111), (200), and (220) corresponding to metallic Cu are shown at 43.3°, 50.4°, and 74.1°, respectively. As shown in Fig. 2(b), furthermore, the significant diffraction peaks indicating the (002) and (111) of CuO appear at 35.5° and 38.7°, respectively, which verifies the occurrence of crystalline CuO. The XRD patterns of C, Cu, and CuO were determined by comparing the results with the corresponding standards, PDF#26-1076, PDF#04-0836, PDF#45-0937, and in Fig. 2(c)-(d).

2. Cyclic Voltammetry Characteristic of the Electrodes

The effect of electrode surface modification with and without analyte was investigated. The electrochemical behavior of AMX was conducted to evaluate its electrochemical activity on carbon-paper substrates. To determine the oxidation behavior of AMX on the electrodes, the cyclic voltammetry (CV) of as-prepared electrodes was obtained in the phosphate buffer solution (PBS) of 0.1 mol L^{-1} at pH 7.0, at a scan rate of 50 mV s^{-1} and a potential range of −1.0 V to +1.0 V (vs. Ag/AgCl) (cf. Fig. 3).

As noticed in Fig. 3(a), no obvious redox signal was recorded when the bare carbon paper was used as an electrode. A slight increase in the current signal can be seen when Ac/Cp electrode is used as in Fig. 3(b). It represents that the activated carbon increases the current. Further enhancement of current intensity in electrochemical response is observed when the electrodes of Cu@Ac/Cp and CuO@Ac/Cp are used. In Fig. 3(c), much enhancement in voltammetric current has been observed on the Cu@Ac/Cp electrode, and it is further providing a sharp increase in the current when the CuO@Ac/Cp has been utilized on the electrode surface (cf. Fig. 3(d)). To some extent, the oxides of copper play an important role in increasing the sensitivity of AMX detection. Namely, the

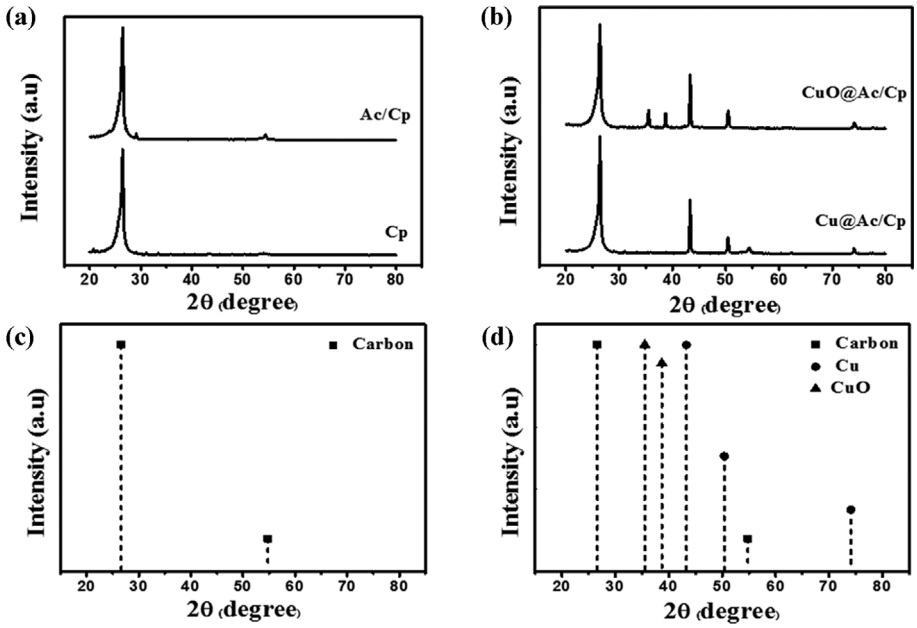

Fig. 2. The XRD analysis of (a) Cp and Ac/Cp, (b) Cu@Ac/Cp and CuO@Ac/Cp. Standard XRD patterns of (c) Carbon, and (d) Cu and CuO.

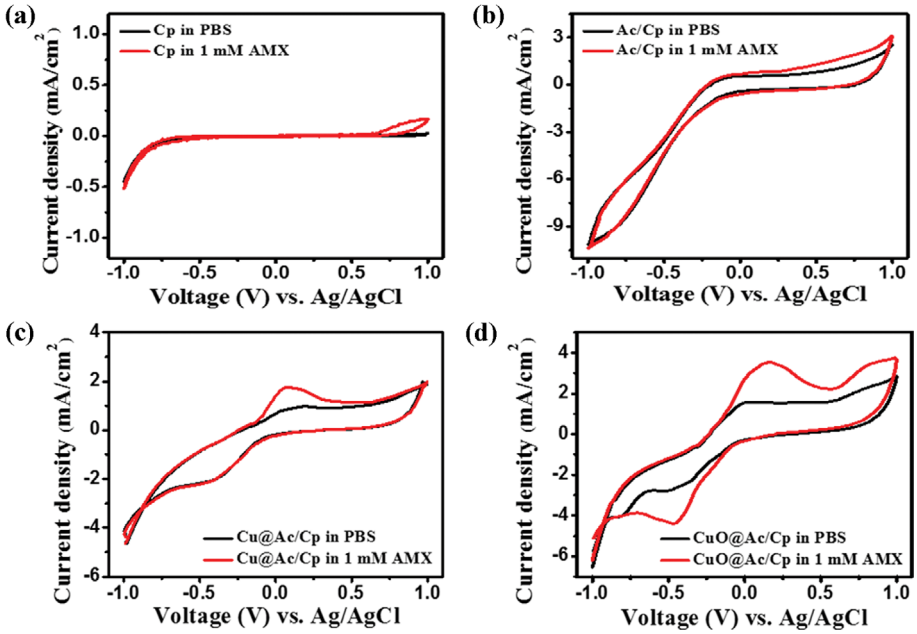

Fig. 3, The CV response of (a) bare Cp, (b) Ac/Cp, (c) Cu@Ac/Cp, and (d) CuO@Ac/Cp in the presence and absence of AMX in phosphate buffer solution (PBS).

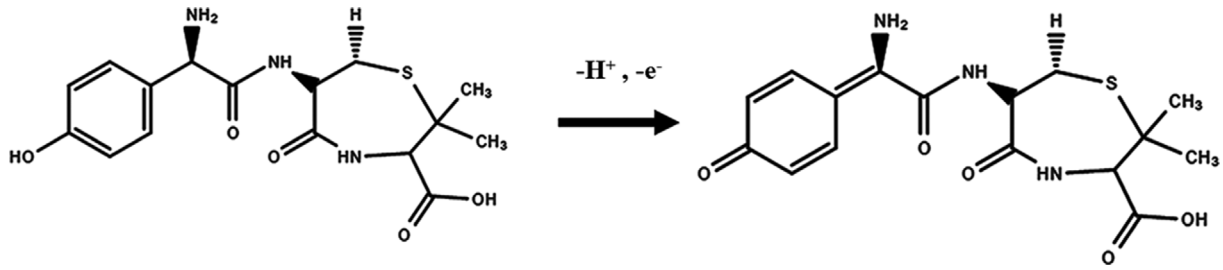

Fig. 4. The electrochemical oxidation process of AMX.

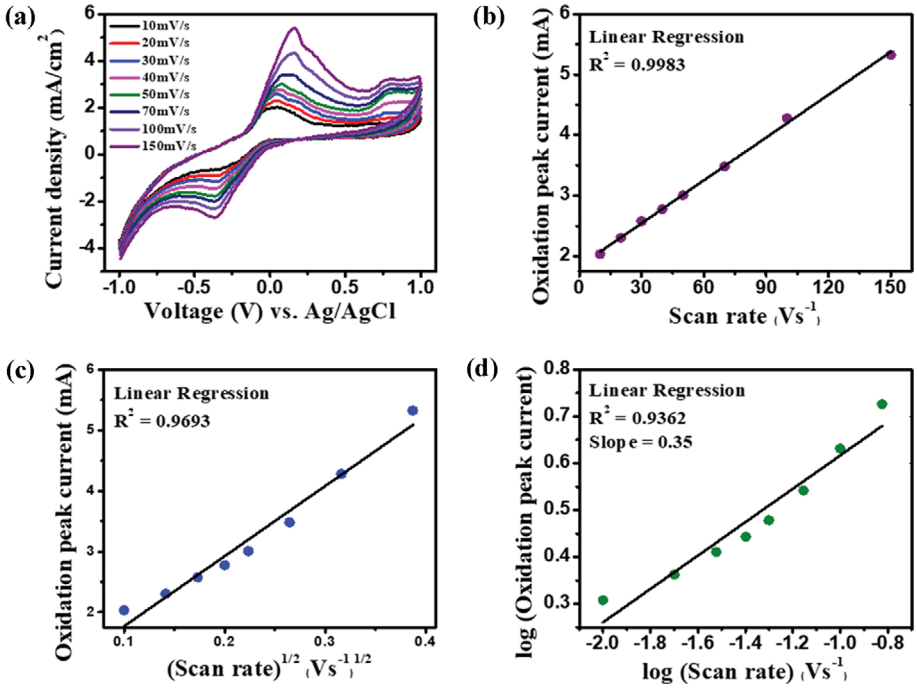

Fig. 5. (a) The effect of different scan rates on cyclic voltammetry at the CuO@Ac/Cp sensor for 1 mM AMX in PBS (pH 7.0); (b) plot of oxidation peak current vs. scan rate; (c) plot of oxidation peak current vs. square root of scan rate; (d) plot of log [oxidation peak current] vs. log [scan rate].

CuO is more favorable in enhancing the sensitivity of the electrochemical sensor in detecting AMX, of which electrochemical reactions correspond to the oxidation of AMX [43]. A schematic diagram of the reaction is presented in Fig. 4 [15].

To investigate the mass transfer mechanism of the redox specimen, the effect of scan rate on CuO@Ac/Cp electrode in PBS at pH 7.0 was monitored as shown in Fig. 5(a). As the scan rate increases from 10 mV/s to 150 mV/s, the peaks of AMX oxidation currents in 0.1 M of PBS (pH 7.0) have moved to more positive values, indicating that the reaction is quasi-reversible. To analyze the mass transport activity of AMX, the oxidation peak current vs. scan rate was also plotted, which is shown in Fig. 5(b). This linear plot indicates that the mass transfer of the analyte on the electrode surface has been controlled by AMX adsorption process [44]. The peak shifting of oxidation current has a linear relationship with the square root of scan rate, as shown in Fig. 5(c), revealing that the mass transport mechanism is limited by diffusion process. For confirmation, the oxidation peak current vs. scan rate was plotted in logarithm scales, as plotted in Fig. 5(d). In this logarithmic plot, a slope represents the characteristics of electrode reaction whether it is a diffusion-controlled or surface adsorption-controlled reaction. In the plot of Fig. 5(d), the slope was fitted to 0.35, which indicated that the reaction was more likely diffusion-controlled [45,46].

The electrochemical oxidation mechanism of AMX was also studied in PBS solution containing 2 mM AMX with various pH values ranging from 5.0 to 9.0. The oxidation peak of AMX gradually shifted towards more negative potential with an increase in pH, indicating deprotonation during the oxidation process at higher pH, as seen in Fig. S3. Fig. S3 (inset) depicts a linear relationship between pH value and AMX oxidation potential with a slope of 47 mV per unit pH. The proton to electron ratio was determined to be 0.8, indicating that the AMX oxidation process involves one electron and one proton as illustrated in Fig. 4.

The changes in CV curves of CuO@Ac/Cp electrodes with different concentration of AMX from 1 mM to 5 mM in 0.1 M PBS at pH 7.0 are presented in Fig. 6. The analytical response shows that better analytical curves are obtained when the CuO@Ac/Cp electrode is used. A linear increase in the oxidation currents is ob-

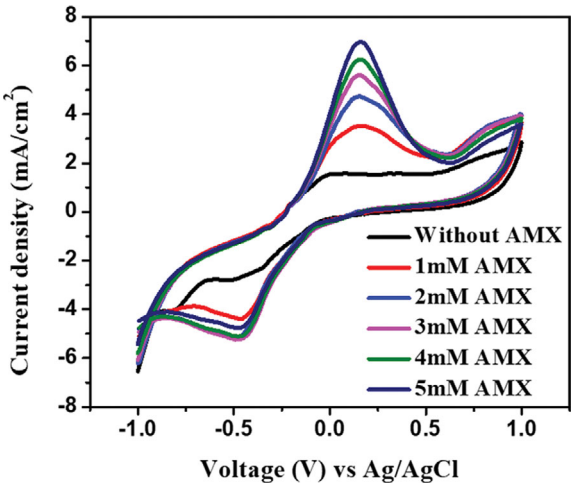

Fig. 6. The effect of different concentrations of AMX on cyclic voltammetry at the CuO@Ac/Cp sensor at 50 mV s^{-1} scan rate in PBS (pH 7.0).

served with increasing the concentration of AMX in the supporting electrolyte. These results indicate significant improvement in AMX sensing performance after modification of the electrode with copper oxides. The voltammograms obtained for the oxidation of AMX on freshly prepared Cu@Ac/Cp and CuO@Ac/Cp electrodes and at the same electrodes after 10, 30, and 60 days of contact with the air are shown in Fig. S1 and Fig. S2, respectively. The oxidation peak potential of both electrodes slightly reduced, even after exposure to the electrolyte. It was then washed, dried, and stored in ambient conditions for 60 days. Furthermore, even after repeated use, the response was found to be stable over several days.

Additionally, we performed interfering studies of AMX in the presence of other chemical compounds such as glucose, urea, and ascorbic acid (AA). Here, Fig. S4 presents the current responses with the baseline correction. AMX was first added to the 0.1 M PBS and the result was recorded, which is shown in Fig. S4(a). All these interfering chemicals were tested separately with AMX at a concentration five times higher than AMX (200 μM) as presented in Fig. S4(b)-(e). Negligible changes have been recorded even after the addition of interfering substances. Fig. S4(f) presents the changes in the oxidation peak current due to the interfering substances, which also confirms the negligible disturbances observed after the addition of chemical compounds.

3. Electrochemical Impedimetric Detection of AMX on CuO@Ac/Cp

For the evaluation of sensing performance on the impedance spectrometric measurements, the AMX has been introduced in the electrochemical system with CuO@Ac/Cp electrodes in a wide range of concentrations from 10 μM to 5 mM. The impedance measurements are presented in Fig. 7(a) and Fig. 7(b), which are the Nyquist plot and the Bode plot, respectively. The obtained result shows that the impedance value increases as the AMX concentration increases. It explains that the electrode is sensing the resistance increment as the concentration of AMX increases.

More careful observation of the detection performance of CuO@Ac/Cp electrode was carried out in two different AMX concentration ranges from 10 μM to 100 μM and from 100 μM to 5 mM, respectively. As shown in Fig. 8, the response of the |Z| value has been divided into two linear ranges with the R^2 values of 0.8927 and 0.9712, of which lines are very well fitted linearly. The increase of the |Z| value of the electrode CuO@Ac/Cp is proportional to the concentration of AMX in two linear ranges, 10 μM to 100 μM and 100 μM to 5 mM, respectively. In the lower concentration range of AMX, the resistance increased sharply, whereas the resistance increased still linearly but much slower in higher concentration ranges. It is due to the differences in surface coverage on the sensor electrode at the time of AMX adsorption. At lower coverages with lower concentrations of AMX, the reaction is limited by diffusion and the sensitivity (i.e., dependency on the concentration) is high. Once the surface coverage reaches the saturation point, however, the surface-reaction rate dominates the sensitivity, result-

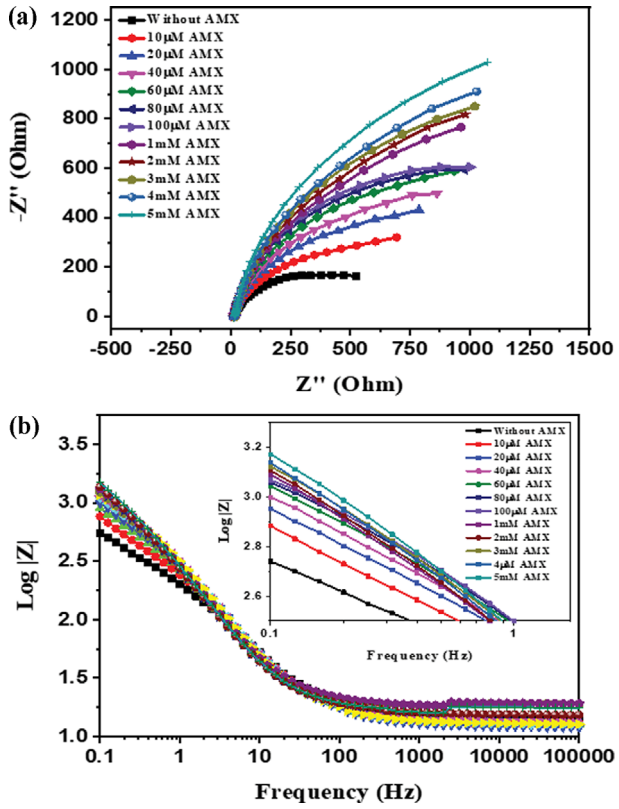

Fig. 7. (a) Nyquist plot and (b) Bode plot of different concentrations of AMX on CuO@Ac/Cp sensor at 0.15 V in PBS (pH 7.0).

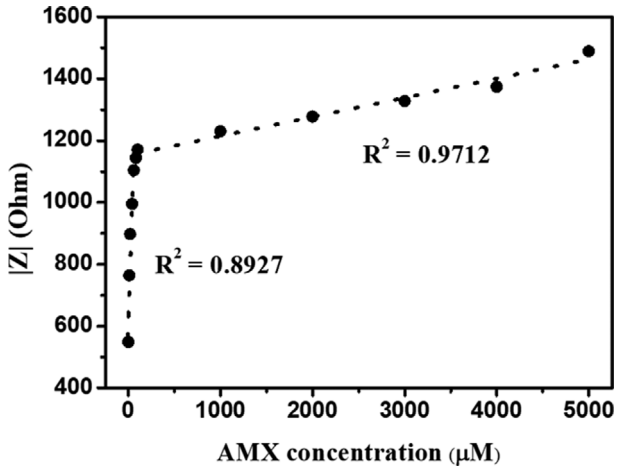

Fig. 8. Effect of AMX concentration on |Z| at 0.1 Hz in PBS (pH 7.0).

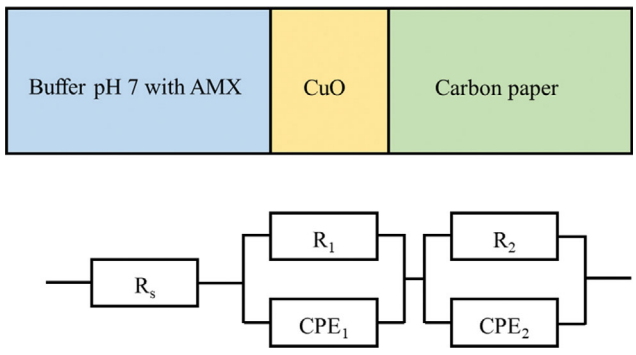

Fig. 9. Schematic diagram of the equivalent circuit.

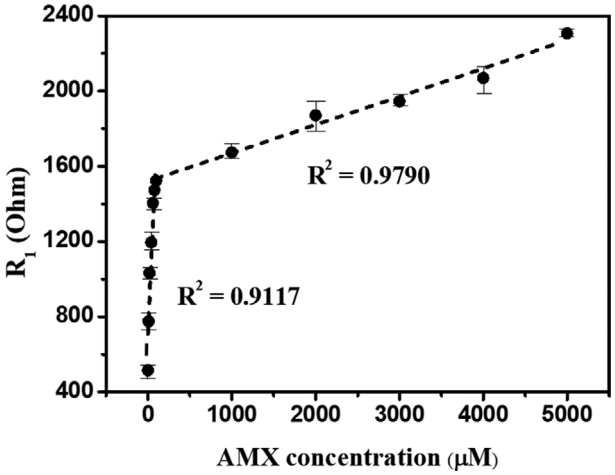

Fig. 10. Effect of AMX concentration on R_1 in PBS (pH 7.0).

ing in a smaller change in the impedance value [47,48].

As shown in Fig. 9, the equivalent circuit was estimated based on a three-electrode system of CuO/Cp in PBS solution at pH 7.0 containing AMX. In Fig. 9, R_s, R_1, and R_2 represent the resistance in AMX solution, charge-transfer resistance value of the CuO layer and the AMX solution, and the response of the carbon paper and CuO layer of the electrode, respectively, whereas CPE_1 and CPE_2 represent the constant-phase elements of active materials and carbon substrate, respectively. With the aid of the software Zman EIS analysis, equivalent circuit fitting was carried out to investigate the interaction between the AMX and the electrode material. The simulation data and fitting results are presented in Table S2. The table clearly shows that R_s, R_2, CPE_1, and CPE_2 do not follow any pattern. R_1, on the other hand, increases gradually with the increase in the concentration of AMX in the system. As the reaction proceeded, the AMX diffused into the CuO layer, and the R_1 increased rapidly from 10 μM to 100 μM concentration of AMX, as shown in the first slope of Fig. 10, due to the high diffusing possibility on the electrode. Once the active materials were filled (higher concentration), the R_1 increased at a much lower rate from 100 μM to 5 mM concentration of AMX, as shown in the second slope. For this reason, the surface coverage reaches a saturation point and blocks further movement of the AMX. Upon fitting, it is found that the resistance of active materials 'R_1' is mainly responsible for the sensing of AMX in solution. To obtain the sensitivity, as shown in Fig. 10, the first linear regression equation was employed and the calculated relation of R_1 and AMX concentration was:

$$R_1=708.9566+9.5528\ [AMX]\ (R^2=0.9117) \quad (1)$$

and

$$R_1=1{,}521.1161+0.1499\ [AMX]\ (R^2=0.9790) \quad (2)$$

From Eqs. (1) and (2), the calculated value of sensitivity was 9.5528 $\Omega\ \mu M^{-1}$ and 0.14994 $\Omega\ \mu M^{-1}$, respectively.

The limit of detection (LOD) was determined using the following equation:

$$LOD=3\ s/m \quad (3)$$

where s is the standard deviation of the five blank tests, and m is the slope.

Table 1 summarizes the comparison of the analytical performance of the AMX determination between the prepared sensor in this work and the other electrochemical sensors in the literature. Overall, the performance of the electrode in terms of LOD in this work reports competitive or superior results as compared to the other recently published research [49-57].

4. Recovery Studies of AMX

To demonstrate the performance of the prepared electrode to determine AMX in practical application, a synthetic urine sample was prepared for impedimetric sensing of AMX in urine, as described in the experimental section. The sensing accuracy and recovery performance after the dose of urine are summarized in Table 2. Even with the AMX in synthetic urine, the accuracy was maintained within errors of 1.7-3.2%, and the sensor electrode recovered about 96.8-98.3%. It suggests that the EIS method can be successfully applied in sensing AMX in the synthetic urine sam-

Table 1. Analytical performance of synthesized electrode compared to relevant electrochemical sensors for AMX determination

Electrode Sensor	Technique	LOD (μM)	Linear range (μM)	Ref.
Modified CPE	SWV	8.49	18.9-91.9	[49]
Ni/Curcumin/CPE	Amperometry	5.0	80-100	[50]
Cu/POT(SDS)/CPE	Amperometry	3.0	5-150	[51]
Glutaraldehyde/GA/GCE	SWV	0.92	2-25	[52]
PNI/CPE	CV	0.812	1-200	[26]
DMBQ/ZnO/CNTs/CPE	SWV	0.5	1-950	[53]
B-Diamond	DPV	0.25	0.5-40	[54]
MWCNT/GCE	CV	0.2	0.6-80	[55]
CB/DPH/GCE	SWV	0.12	2-18.8	[56]
PGA/3D-GE/GCE	SWV	0.118	20-60	[57]
QDs-P6LC-PEDOT:PSS/GCE	SWV	0.05	0.90-69	[15]
CuO@Ac/Cp	EIS	0.174	10-100	This work

SWV=Square Wave Voltammetry, CV=Cyclic Voltammetry, DPV=Differential Pulse Voltammetry, EIS=Electrochemical Impedance Spectroscopy

Table 2. The determination results of sensing accuracy on detection of AMX and recovery rate after being exposed to AMX-contained synthetic urine

Sample	Added (μM)	Found[a] (μM)	Recovery[b] (%)	RSD[c] (%)
Synthetic urine	0	0	100	0
	25	24.2	96.8	3.06
	75	73.7	98.3	2.41

[a]Average of three measured concentrations. [b]Recover (%)=[Found/Added]×100. [c]Relative standard deviation=[Standard deviation/mean]×100.

ple, and the improved electrode in this work can be used to accurately determine AMX.

CONCLUSIONS

CuO-based electrode has been fabricated using a simple spray coating technique that allows the sensor to exhibit high analytical characteristics, especially in terms of sensitivity, accuracy, and repeatability. The CuO@Ac/Cp electrode shows high sensitivity and excellent selectivity for the determination of AMX concentration. The particles of annealed CuO exhibit a high redox-current response in cyclic voltammetry. Impedimetric performance of CuO@Ac/Cp has been investigated in a wide range of AMX concentration, and the changes of impedance values were linear in two dynamic ranges from 10 μM to 100 μM and from 1 mM to 5 mM, in which the sensitivity was calculated as 9.5528 Ω μM^{-1} and 0.1499 Ω μM^{-1}, respectively. The proposed CuO@Ac/Cp based sensor could be a promising platform for the impedimetric detection of AMX for sensing applications, due to its simple electrode preparation steps and effective sensing performance.

ACKNOWLEDGEMENTS

This research was supported by the National Research Foundation of Korea (NRF) grant funded by the Korea government (MSIT) [Grant number NRF-2021R1A4A1024129].

ORCID

Chan-Hwa Chung: https://orcid.org/0000-0003-2808-1001.

SUPPORTING INFORMATION

Additional information as noted in the text. This information is available via the Internet at http://www.springer.com/chemistry/journal/11814.

REFERENCES

1. J. P. Swann, *Br. J. Hist. Sci.*, **16**, 154 (1983).
2. A. Hrioua, A. Loudiki, A. Farahi, M. Bakasse, S. Lahrich, S. Saqrane and M. A. El Mhammedi, *Bioelectrochemistry*, **137**, 107687 (2021).
3. R. Sutherland, *Microbiology*, **34**, 85 (1964).
4. M. G. El-sayed, A. A. El-komy, A. E. Elbarawy and G. E. Mustafa, *J. Phys. Pharm. Adv.*, **4**, 515 (2014).
5. S. Mathur, A. Fuchs, J. Bielicki, J. Van Den Anker and M. Sharland, *Paediatr. Int. Child Health*, **38**, S66 (2018).
6. J. Fernández, I. A. C. Ribeiro, V. Martin, O. L. Martija, E. Zuza, A. F. Bettencourt and J.-R. Sarasua, *Mater. Sci. Eng.: C*, **93**, 529 (2018).
7. K. Kümmerer, *Chemosphere*, **75**, 417 (2009).
8. H. Mansouri, R. J. Carmona, A. Gomis-Berenguer, S. Souissi-Najar, A. Ouederni and C. O. Ania, *J. Colloid Interface Sci.*, **449**, 252 (2015).
9. G. Yang and F. Zhao, *Electrochim. Acta*, **174**, 33 (2015).
10. F. A. O. Joint and W. H. Organization, W. H. O. E. C. on Food Additives, and others, *Toxicological evaluation of certain veterinary drug residues in food: prepared by the seventy-fifth meeting of the Joint FAO/WHO Expert Committee on Food Additives (JECFA)*, World Health Organization (2012).
11. R. A. Figueroa and A. A. MacKay, *Environ. Sci. Technol.*, **39**, 6664 (2005).
12. N. Erdinç, S. Göktürk and M. Tunçay, *Colloids Surf. B: Biointerfaces*, **75**, 194 (2010).
13. H. Wang, N. Wang, B. Wang, Q. Zhao, H. Fang, C. Fu, C. Tang, F. Jiang, Y. Zhou, Y. Chen and Q. Jiang, *Environ. Sci. Technol.*, **50**, 2692 (2016).
14. G. O. Androga, D. R. Knight, S.-C. Lim, N. F. Foster and T. V. Riley, *Anaerobe*, **54**, 55 (2018).
15. A. Wong, A. M. Santos, F. H. Cincotto, F. C. Moraes, O. Fatibello-Filho and M. D. P. T. Sotomayor, *Talanta*, **206**, 120252 (2020).
16. K. M. Matar, *Chromatographia*, **64**, 255 (2006).
17. L. Sun, L. Jia, X. Xie, K. Xie, J. Wang, J. Liu, L. Cui, G. Zhang, G. Dai and J. Wang, *Food Chem.*, **192**, 313 (2016).
18. G. Pajchel, K. Pawłowski and S. Tyski, *J. Pharm. Biomed. Anal.*, **29**, 75 (2002).
19. A. Garcia-Reiriz, P. C. Damiani and A. C. Olivieri, *Talanta*, **71**, 806 (2007).
20. R. H. Barbhaiya, P. Turner and E. Shaw, *Clin. Chim. Acta*, **77**, 373 (1977).
21. F. A. Aly, N. A. Alarfaj and A. A. Alwarthan, *Anal. Chim. Acta*, **414**, 15 (2000).
22. A. P. Ball, P. G. Davey, A. M. Geddes, I. D. Farrell and G. R. Brookes, *The Lancet*, **315**, 620 (1980).
23. D. Krasucka, C. Kowalski, M. Osypiuk and G. Opielak, *Acta Chromatographica*, **27**, 55 (2015).
24. M. Akhond, G. Absalan and H. Ershadifar, *Spectrochim. Acta Part A: Mol. Biomolec. Spectr.*, **143**, 223 (2015).
25. D. C. Napoleão, R. B. Pinheiro, L. E. M. C. Zaidan, J. M. Rodriguez-Diaz, A. da N. Araújo, M. da C. Montenegro and V. L. da Silva, *Desalination Water Treatment*, **57**, 10988 (2016).

26. B. Uslu and I. Biryol, *J. Pharm. Biomed. Anal.*, **20**, 591 (1999).
27. A. K. Jain, V. K. Gupta, L. P. Singh and J. R. Raisoni, *Electrochim. Acta*, **51**, 2547 (2006).
28. P. Norouzi, V. K. Gupta, B. Larijani, M. R. Ganjali and F. Faridbod, *Talanta*, **127**, 94 (2014).
29. S. Cheemalapati, B. Devadas and S.-M. Chen, *J, Colloid Interface Sci.*, **418**, 132 (2014).
30. V. K. Gupta, N. Mergu, L. K. Kumawat and A. K. Singh, *Talanta*, **144**, 80 (2015).
31. A. Muhammad, N. A. Yusof, R. Hajian and J. Abdullah, *Sensors*, **16**, 56 (2016).
32. Z. Guo, D.-D. Li, X.-K. Luo, Y.-H. Li, Q.-N. Zhao, M.-M. Li, Y.-T. Zhao, T.-S. Sun and C. Ma, *J. Colloid Interface Sci.*, **490**, 11 (2017).
33. Z. Shamsadin-Azad, M. A. Taher, S. Cheraghi and H. Karimi-Maleh, *J. Food Meas. Charact.*, **13**, 1781 (2019).
34. H. Karimi-Maleh, M. Sheikhshoaie, I. Sheikhshoaie, M. Ranjbar, J. Alizadeh, N. W. Maxakato and A. Abbaspourrad, *New J. Chem.*, **43**, 2362 (2019).
35. H. Karimi-Maleh and O. A. Arotiba, *J. Colloid Interface Sci.*, **560**, 208 (2020).
36. D. P. dos Santos, M. F. Bergamini and M. V. B. Zanoni, *Int. J. Electrochem. Sci.*, **5**, 1399 (2010).
37. A. Hrioua, A. Farahi, S. Lahrich, M. Bakasse, S. Saqrane and M. A. El Mhammedi, *ChemistrySelect*, **4**, 8350 (2019).
38. S. J. Lyle and S. S. Yassin, *Anal. Chim. Acta*, **274**, 225 (1993).
39. M.-H. Chiu, J.-L. Chang and J.-M. Zen, *Electroanalysis: An international j. devoted to fundamental and practical aspects of electroanalysis*, Wiley-VCH, New York (2009).
40. M. T. Feroze, S. K. Sami, D. Doonyapisut, B. Kim and C.-H. Chung, *ChemElectroChem*, **7**, 730 (2020).
41. K. Zhuo, C. Y. An, P. K. Kannan, N. Seo, Y.-S. Park and C.-H. Chung, *Korean J. Chem. Eng.*, **34**, 1483 (2017).
42. Y.-S. Park, C. Y. An, P. K. Kannan, N. Seo, K. Zhuo, T. K. Yoo and C.-H. Chung, *Appl. Surf. Sci.*, **389**, 865 (2016).
43. T. M. Prado, F. H. Cincotto, F. C. Moraes and S. A. S. Machado, *Electroanalysis*, **29**, 1278 (2017).
44. N. Elgrishi, K. J. Rountree, B. D. McCarthy, E. S. Rountree, T. T. Eisenhart and J. L. Dempsey, *J. Chem. Educ.*, **95**, 197 (2018).
45. A. J. Bard and L. R. Faulkner, *Electrochemical methods: Fundamentals and applications*, 2nd Edition, Wiley-VCH, New York (2001).
46. E. Chrzescijanska, E. Wudarska, E. Kusmierek and J. Rynkowski, *J. Electroanal. Chem.*, **713**, 17 (2014).
47. G. Bhattacharya, A. Mathur, S. Pal, J. McLaughlin and S. S. Roy, *Int. J. Electrochem. Sci.*, **11**, 6370 (2016).
48. C. Tlili, K. Reybier, A. Géloën, L. Ponsonnet, C. Martelet, H. Ben Ouada, M. Lagarde and N. Jaffrezic-Renault, *Anal. Chem.*, **75**, 3340 (2003).
49. M. F. Bergamini, M. F. S. Teixeira, E. R. Dockal, N. Bocchi and E. T. G. Cavalheiro, *J. Electrochem. Soc.*, **153**, E94 (2006).
50. R. Ojani, J.-B. Raoof and S. Zamani, *Bioelectrochemistry*, **85**, 44 (2012).
51. B. Norouzi and T. Mirkazemi, *Russian J. Electrochem.*, **52**, 37 (2016).
52. D. P. Santos, M. F. Bergamini and M. V. B. Zanoni, *Sens. Actuators B: Chem.*, **133**, 398 (2008).
53. H. Karimi-Maleh, F. Tahernejad-Javazmi, V. K. Gupta, H. Ahmar and M. H. Asadi, *J. Mol. Liq.*, **196**, 258 (2014).
54. Ľ. Švorc, J. Sochr, M. Rievaj, P. Tomčík and D. Bustin, *Bioelectrochemistry*, **88**, 36 (2012).
55. B. Rezaei and S. Damiri, *Electroanalysis*, **21**, 1577 (2009).
56. P. B. Deroco, R. C. Rocha-Filho and O. Fatibello-Filho, *Talanta*, **179**, 115 (2018).
57. C. Chen, X. Lv, W. Lei, Y. Wu, S. Feng, Y. Ding, J. Lv, Q. Hao and S.-M. Chen, *Anal. Chim. Acta*, **1073**, 22 (2019).